

Single transmission-line readout method for silicon photomultiplier based time-of-flight and depth-of-interaction PET

This content has been downloaded from IOPscience. Please scroll down to see the full text.

2017 Phys. Med. Biol. 62 2194

(<http://iopscience.iop.org/0031-9155/62/6/2194>)

View [the table of contents for this issue](#), or go to the [journal homepage](#) for more

Download details:

IP Address: 147.46.96.91

This content was downloaded on 28/07/2017 at 06:18

Please note that [terms and conditions apply](#).

You may also be interested in:

[Delay grid multiplexing: simple time-based multiplexing and readout method for silicon photomultipliers](#)

Jun Yeon Won, Guen Bae Ko and Jae Sung Lee

[Development of capacitive multiplexing circuit for SiPM-based time-of-flight \(TOF\) PET detector](#)

Hyeok-Jun Choe, Yong Choi, Wei Hu et al.

[Time-over-threshold for pulse shape discrimination in a time-of-flight phoswich PET detector](#)

Chen-Ming Chang, Joshua W Cates and Craig S Levin

[Advances in coincidence time resolution for PET](#)

Joshua W Cates and Craig S Levin

[Achieving fast timing performance with multiplexed SiPMs](#)

M F Bieniosek, J W Cates and C S Levin

[LaBr₃:Ce and SiPMs for time-of-flight PET](#)

Dennis R Schaart, Stefan Seifert, Ruud Vinke et al.

[A novel depth-of-interaction block detector for positron emission tomography using a dichotomous orthogonal symmetry decoding concept](#)

Yuxuan Zhang, Han Yan, Hossain Baghaei et al.

 **RayStation**
HARMONIZE YOUR
TREATMENT PLANNING

INTRODUCING
RAYSTATION 6
WITH SUPPORT FOR
TOMOTHERAPY*

*Subject to regulatory clearance in some markets.

Single transmission-line readout method for silicon photomultiplier based time-of-flight and depth-of-interaction PET

Guen Bae Ko^{1,2} and Jae Sung Lee^{1,2,3,4,5}

¹ Department of Nuclear Medicine, Seoul National University College of Medicine, Seoul 03080, Korea

² Department of Biomedical Sciences, Seoul National University College of Medicine, Seoul 03080, Korea

³ Interdisciplinary Program in Radiation Applied Life Science, Seoul National University College of Medicine, Seoul 03080, Korea

⁴ Institute of Radiation Medicine, Medical Research Center, Seoul National University College of Medicine, Seoul 03080, Korea

E-mail: jaes@snu.ac.kr

Received 3 October 2016, revised 10 January 2017

Accepted for publication 18 January 2017

Published 21 February 2017



CrossMark

Abstract

We propose a novel single transmission-line readout method for whole-body time-of-flight positron emission tomography applications, without compromising on performance. The basic idea of the proposed multiplexing method is the addition of a specially prepared tag signal ahead of the scintillation pulse. The tag signal is a square pulse that encodes photon arrival time and channel information. The 2D position of a silicon photomultiplier (SiPM) array is encoded by the specific width and height of the tag signal. A summing amplifier merges the tag and scintillation signals of each channel, and the final output signal can be acquired with a one-channel digitizer. The feasibility and performance of the proposed method were evaluated using a 1:1 coupled detector consisting of 4×4 array of LGSO crystals and 16 channel SiPM. The sixteen 3 mm LGSO crystals were clearly separated in the crystal-positioning map with high reliability. The average energy resolution and coincidence resolving time were $11.31 \pm 0.55\%$ and 264.7 ± 10.7 ps, respectively. We also proved that the proposed method does not degrade timing performance with increasing multiplexing ratio. The two types of LGSO crystals ($L_{0.95}$ GSO and $L_{0.20}$ GSO) in phoswich detector were also clearly identified with the high-reliability using pulse shape discrimination,

⁵ Author to whom any correspondence should be addressed.

thanks to the well-preserved pulse shape information. In conclusion, the proposed multiplexing method allows decoding of the 3D interaction position of gamma rays in the scintillation detector with single-line readout.

Keywords: silicon photomultiplier (SiPM), time-of-flight (TOF), depth-of-interaction (DOI), signal multiplexing, block detector

(Some figures may appear in colour only in the online journal)

1. Introduction

Time-of-flight (TOF) information is required in modern whole-body positron emission tomography (PET) systems because it improves the signal-to-noise ratio (SNR) and reduces image artifacts (Conti 2010, 2011, Conti *et al* 2013, Lee and Kim 2014, Surti 2015, Ullah *et al* 2016). The gain in the SNR can be estimated from the coincidence resolving time (CRT: the measurement accuracy of the photon arrival time of two annihilated gamma rays). To achieve good CRT, the PET detector should have high photon counting statistics, fast time response, and low noise. In this respect, the combination of novel fast and bright scintillation crystals and brand-new low noise silicon photomultipliers (SiPMs) is optimal to obtain accurate TOF information. The SiPM is a semiconductor photosensor with reasonably high photon detection efficiency, fast response time, and magnetic field insensitivity. The previous studies on SiPM highlighted its magnetic resonance imaging (MRI) compatibility for PET/MRI applications (Yamamoto *et al* 2012, Yoon *et al* 2012, Nishikido *et al* 2014, Olcott *et al* 2015, Kang *et al* 2015, Wehner *et al* 2015, Becker *et al* 2016, Jung *et al* 2016, Ko *et al* 2016a, 2016b) and fast time response for TOF PET (Gundacker *et al* 2013, Seifert *et al* 2013, Schmall *et al* 2014, Miller *et al* 2015, Neill and Jackson 2015, Levin *et al* 2016). Moreover, the small size of the SiPM enables one-to-one (1:1) coupling of scintillators and photosensors which offers the best PET detector performance by minimizing the loss of optical photons from the scintillation crystals.

In the last few years, several studies have broken through the wall of 200 ps CRT by means of 1:1 coupling of an SiPM and a 20 mm-long crystal, the size relevant to clinical TOF PET (Cates *et al* 2015, Nemallapudi *et al* 2015, Seifert and Schaart 2015, Cates and Levin 2016). However, maintaining this good CRT at system level remains challenging because handling the many readout channels from multiple SiPM pixels without compromising performances is such a difficult task.

Although the individual readout of SiPM pixels using analog-to-digital converters (ADCs) would offer optimized energy resolution, CRT, and count rate performance, it is not a practical solution because of its high cost and large volume. Charge division multiplexing is an efficient method to reduce the number of readout channels, but results in poor CRT due to its increasing capacitance and accumulating dark current for a large number of SiPMs (Song *et al* 2010, Downie *et al* 2013, Ko *et al* 2013, Liu *et al* 2014). A time-based readout such as time-over-threshold (Powolny *et al* 2011, Shimazoe *et al* 2012, Grant and Levin 2014) is a possible solution to read out SiPM pixels individually at an affordable cost. This is because the signals can be read out by multi-channel time-to-digital converters implemented in a field-programmable gate array instead of the high-cost ADCs (Traxler *et al* 2011, Aguilar *et al* 2015, Liu and Wang 2015, Won *et al* 2015). However, it lacks scintillation pulse information, which is crucial for acquiring accurate energy information and providing capability for depth-of-interaction (DOI) encoding by pulse shape discrimination (PSD) (Schmand *et al* 1998, Pepin *et al* 2004, Roncali *et al* 2012). The DOI encoding capability is another key technique

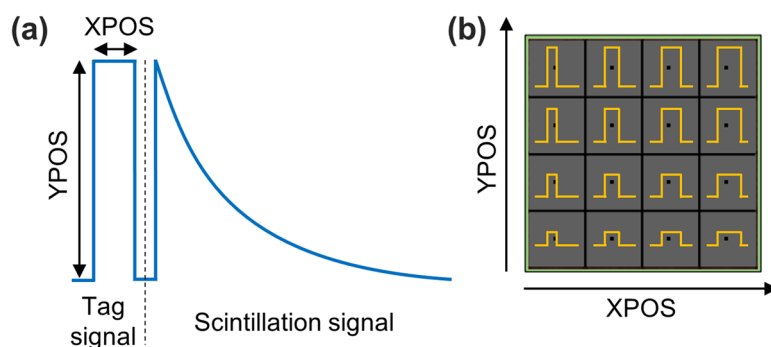


Figure 1. Concept of PTM. (a) Waveform of PTM consisting of tag signal and scintillation signal and (b) example of tag signal for 4×4 SiPM array.

for next-generation PET systems because it allows the improvement of both spatial and time resolution by reducing parallax error and compensating for the light transfer time difference in scintillation crystals (Ito *et al* 2011).

In this paper, we propose a new signal multiplexing technique suitable for 1:1 coupled SiPM detectors. The proposed method requires only one channel digitizer to obtain information of the gamma-ray event including incident position, deposited energy, and arrival time. In this study, we have investigated whether the proposed method does not compromise CRT with increasing multiplexing ratio while it preserves the scintillation pulse information, offering the capability of simultaneous estimations of TOF and DOI information.

2. Materials and methods

2.1. Concept of pulse-tagging multiplexing (PTM)

The signal from the photosensor in the scintillation detector (scintillation signal) contains the information on the energy and arrival time of the incident gamma ray, but does not indicate where the photosensor is located. The basic idea of the proposed multiplexing method, PTM, is the addition of a specially prepared tag signal ahead of the scintillation signal (figure 1(a)). The tag signal is a square pulse with a specific width and height representing the position of firing SiPM in the sensor array. The arrival time of the photon is encoded in the rising edge of the tag signal. Using the tag signal that has a height of M steps and a width of N steps, each pixel of the $M \times N$ array SiPM matrix can be distinguished. Figure 1(b) shows an example of tag signals for a 4×4 array.

2.2. Circuit implementation for 16 channel SiPM

We applied the PTM method to a 4×4 SiPM array composed of $3 \times 3 \text{ mm}^2$ photosensitive pixels, with $50 \mu\text{m}$ microcells (3.2 mm pitch; S12642-0404PB-50; Hamamatsu Photonics KK, Japan). Figure 2 shows a schematic drawing of the PTM circuit implemented for the 16 channel SiPM.

The 16 cathodes of the SiPM were bound to the common line (common cathode signal) and magnified through a high-speed current feedback operational amplifier (AD8000; Analog Devices, USA) without signal shaping to generate the scintillation signal part. The individual anodes were passed through passive high pass filters with pole-zero cancellation and

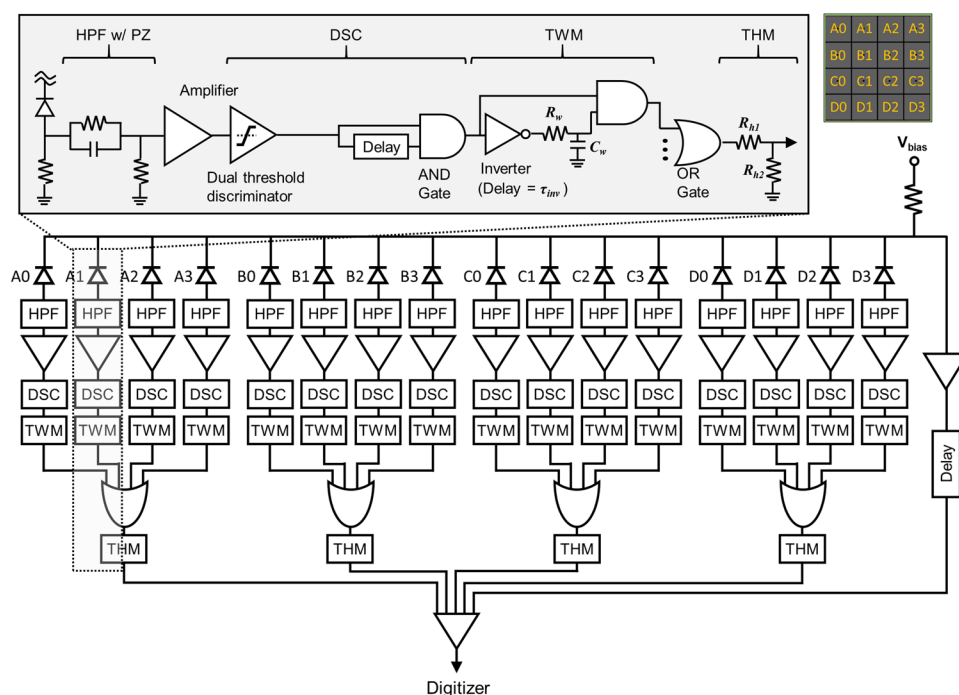


Figure 2. Schematic representation of the PTM circuit implemented for the 16 channel SiPM. HPF = high pass filter; DSC = discriminator; TWM = tag width modulator; THM = tag height modulator.

amplified. The high pass filter was adopted to filter out baseline fluctuations for improving the CRT (Gola *et al* 2013). Digital trigger signals were generated from the amplified anode signals using leading edge discriminators operated with dual threshold. If the input signal exceeds the low threshold (Th_{low}), the leading edge discriminator generates logically high output signal that continues until the input signal falls below the high threshold (Th_{high}) (Grant and Levin 2014). The Th_{low} and Th_{high} were set to 10 mV ($\sim 2\%$ of 511 keV pulse peak) and 100 mV ($\sim 20\%$), respectively.

The position signals share a readout channel in this multiplexing scheme. Therefore, occurrences of two or more events at the same time can cause positioning errors. Thus, we added rejection circuits to the discriminators, which filter out the false triggering events such as dark count and optical cross talk between neighboring crystals. The rejection circuit was implemented using an inverter chain and AND gate (DSC in figure 2). For the 511 keV gamma ray event, which had enough pulse height, the discriminator generated an output signal that had long pulse width. Since the pulse width was longer than the inverter chain delay, the AND gate generated an output signal with shortened pulse width. On the contrary, the false triggering events generated square pulses that had a width shorter than the inverter chain delay, so these events were discarded in the AND gate. This rejection circuit made it possible to avoid a mispositioning situation and improved counting rate performance.

The filtered digital trigger signals were fed into tag width modulators (TWMs). Then the TWM output signals from the cells located on the same row were merged by an OR gate, and the output was fed into the tag height modulator (THM). The TWM (figure 2), consisting of an inverter (intrinsic delay = τ_{inv}), AND gate, resistor (R_w), and capacitor (C_w), adjusted pulse width as a function of RC delay ($\tau_{inv} + \alpha R_w C_w$). The THM (figure 2) was a simple voltage

divider consisting of two resistors (R_{h1} and R_{h2}), which adjusted pulse height as the ratio of their resistance ($R_{h2}/(R_{h1} + R_{h2})$). Thus, the width and height of the tag signal were easily controlled by the capacitor (C_w) and resistor (R_{h2}), respectively.

Finally, a summing amplifier merged the outputs of the THMs and the 50 ns-delayed common cathode signal to avoid interference between tag and scintillation signals. The final output signal can be read only with the one-channel digitizer and the gamma-ray interaction position and arrival time can be calculated from the tag signal part. Since the tag signal was individually generated in each SiPM channel, the timing performance was not degraded by the accumulating dark count and capacitance, which are inevitable in the traditional charge-sharing multiplexing methods.

2.3. Determination of tag signal width and height

In order to distinguish the SiPM pixels in the 2D position map, the step of tag signal width and height should be set sufficiently larger than the spread of measured values in full-width-at-half-maximum (FWHM). Thus, we evaluated the mean and spread of the width and height of the measured tag signal for several different capacitor (C_w) and resistor (R_{h2}) values of the TWM and THM circuits. For evaluation of the TWM, we fixed $R_w = R_{h1} = R_{h2} = 51 \Omega$, while the C_w varied from 1 pF to 1000 pF. For the THM, we fixed C_w to 100 pF and R_w and R_{h1} to 51Ω while the R_{h2} varied from 10 to 51Ω .

The output tag signal was digitized by a high bandwidth digital oscilloscope (DSO9404A, 4 channels \times 10 GS s^{-1} sampling speed, 4 GHz analog bandwidth, 8 bit amplitude resolution; Keysight Technologies, USA). In each condition, 2000-measured pulse samples were analyzed.

Based on the experimental result, $R_w = R_{h1} = 51 \Omega$, $R_{h2} = 10, 12, 15, \text{ and } 17 \Omega$, $C_w = 20, 40, 60, \text{ and } 80 \text{ pF}$ were used for TWM and THM. Using this setting, the PTM circuit encoded the four rows of the SiPM array with an amplitude of approximately 350, 400, 480, and 530 mV and the four columns with a width of approximately 3, 4, 5, and 6 ns, respectively.

2.4. Block detector configuration and experimental setup for PTM evaluation

The performance of PTM circuit was evaluated using a 4×4 $L_{0.95}\text{GSO}$ array ($\text{Lu}_{1.9}\text{Gd}_{0.1}\text{SiO}_4\text{:Ce}$; $3 \times 3 \times 20 \text{ mm}^3$, 3.2 mm pitch), whose pixel and pitch sizes are matched to those of the S12642-0404PB-50 SiPM. The surface of each crystal pixels was polished and wrapped in enhanced specular reflectors (3M, USA). Optical grease (BC-630, Oken, Japan) was used for coupling the SiPM and crystal array.

Coincidence data were acquired with a reference detector consisting of a single $L_{0.95}\text{GSO}$ crystal ($3 \times 3 \times 20 \text{ mm}^3$) and an SiPM (S12642-0404PB-50) having a known single timing resolution of 163 ps, as shown in figure 3. The signal from the reference detector was amplified (gain = 10 V/V) and fed into two second-stage amplifiers: a low gain amplifier (gain = 1) for energy channel and a high gain amplifier (gain = 5) for timing channel. The PTM and reference detector were placed 25 cm away from each other in a thermostatic chamber (20 °C) and irradiated by a 26.8 μCi ^{22}Na point source placed at the center of two detectors. Both SiPMs used for PTM and the reference detector were operated at 4.0 V above their breakdown voltage.

The performance of the PTM detector was also evaluated at different single count rates. Three different single count rates (10, 50, and 250 kcps) were yielded by changing the distance between the PTM detector and 2.1 mCi ^{68}Ge source. Meanwhile, a conventional multiplexing method that shares the anodes to generate energy, time, and position signal (called

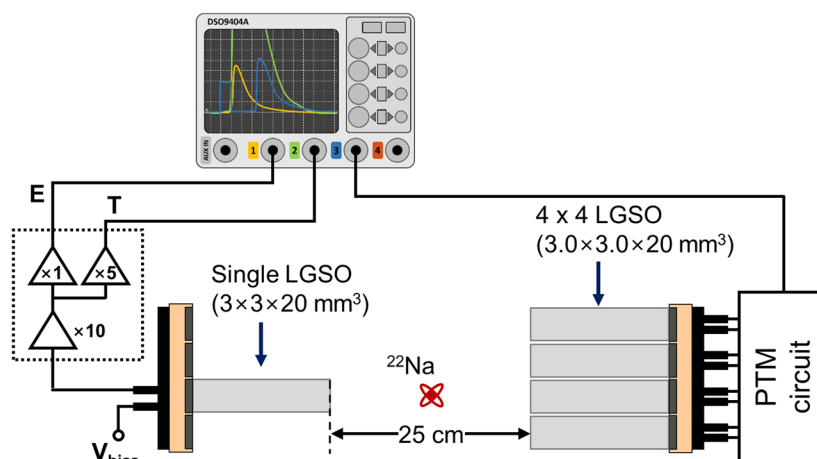


Figure 3. Experimental and data acquisition setup for PTM circuit evaluation.

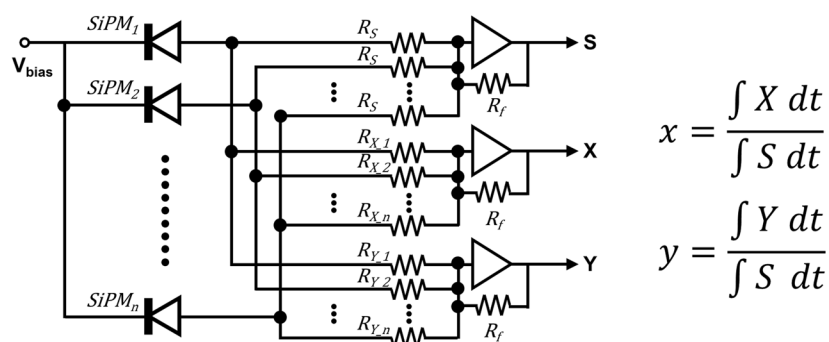


Figure 4. Electrical schematic of the charge-sharing detector used for the comparison.

‘charge sharing’ in this paper) was also evaluated. Figure 4 shows the schematic of the charge-sharing detector used in this experiment. The energy and time information (S in figure 4) were obtained by summing every anode signal, and the X and Y position signals were defined by a weighted sum of the anode signals.

2.5. Data acquisition and analysis

The one channel output of PTM detector and the energy and timing channels of the reference detector were acquired using a digital oscilloscope with 10 GHz sampling speed (DSO9404A), which is the same device used in tag signal width and height evaluation (section 2.3). The tag signal width was calculated as the time difference between the rising and falling edges of tag signal determined at 50% reference level. The tag signal height was calculated as the average voltage of the tag signal. Based on the measured width and height of each tag signal, we composed a 2D map where the x axis is the tag signal width and the y axis is the tag signal height. As a figure-of-merit of the pixel separation, distance to width ratio (DWR) was calculated (Ko and Lee 2015).

The energy of the PTM detector was calculated by integration of the scintillation signal. The arrival times were calculated from the digitalized pulse after linear interpolation by a factor of 10 (i.e. 20 ps resolution). For the PTM detector, the arrival time was determined at the

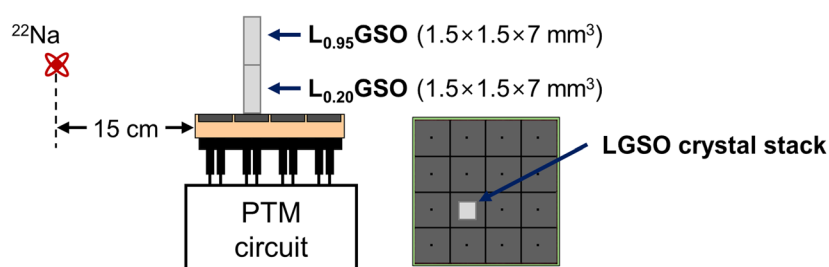


Figure 5. Experimental setup for phoswich detector evaluation.

rising edge of the tag signal. The photon's arrival time at the reference detector was calculated using a digital leading edge discrimination method with 2% threshold from the timing channel signal after event-by-event baseline correction (Ko and Lee 2015).

The coincidence time resolution between PTM and reference detectors was calculated by a Gaussian fitting on the time difference spectrum. The CRT of the PTM detector was then calculated by quadratically subtracting the single time resolution of the reference detector from the time resolution with reference detector and multiplying by $\sqrt{2}$. Only the events within a full-width-at-tenth-of-maximum of 511 keV energy peak were used for the CRT analysis.

2.6. Performance with increasing multiplexing ratio

The CRT of the PTM circuit was evaluated for 1:1, 2:1, 4:1, 8:1 and 16:1 multiplexing ratios. Single $L_{0.95}\text{GSO}$ crystal ($3 \times 3 \times 20 \text{ mm}^3$) was coupled to the PTM circuit for this evaluation. The coincidence data were acquired using the same experimental setup and conditions used for block detector evaluation. For the comparison, the charge sharing method was also evaluated for the same multiplexing ratios.

2.7. Evaluation of phoswich detector

To show the feasibility of the DOI measurement using PSD, a stack of two LGSO crystals ($1.5 \times 1.5 \times 7 \text{ mm}^2$ each) which have different levels of lutetium content was coupled with the center of the SiPM pixel. The $L_{0.2}\text{GSO}$ ($\text{Lu}_{0.4}\text{Gd}_{1.6}\text{SiO}_4:\text{Ce}$, $\tau = 60 \text{ ns}$) crystal was attached to the SiPM pixels and the $L_{0.95}\text{GSO}$ ($\tau = 60 \text{ ns}$) was stacked on the $L_{0.2}\text{GSO}$ because $L_{0.95}\text{GSO}$ produces more light output. The detector was irradiated by ^{22}Na point source from the side of the detector as shown in figure 5. The ratio of tail integration to head integration was calculated from the scintillation signal to distinguish the photon interaction layer. The integration ranges for head and tail integrations were carefully selected to minimize the identification error and they are shown in figure 6.

3. Results

3.1. Pulse property of PTM circuit

Figure 6 shows a representative output pulse of the PTM detector at the center pixel sampled using the oscilloscope (tag signal width $\sim 5 \text{ ns}$ and tag signal height $\sim 400 \text{ mV}$).

Both the tag signal width and height were increased as the C_w and R_{h2} were increased as expected (figure 7). The average spreads of the measured width and height were $79.7 \pm 3.7 \text{ ps}$ and $8.1 \pm 0.8 \text{ mV FWHM}$ respectively, which are the minimum spacing of the width and

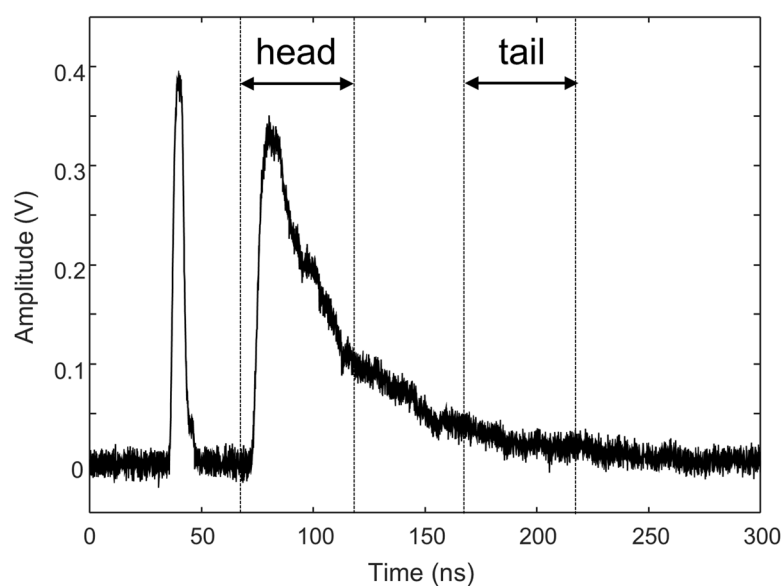


Figure 6. Representative output signal of PTM detector.

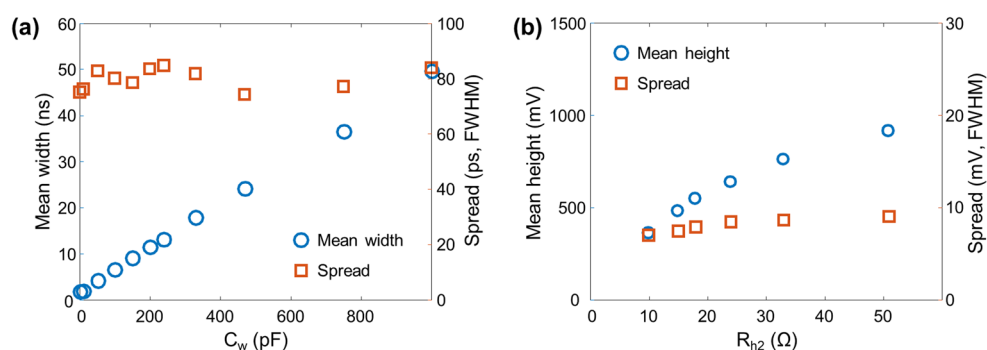


Figure 7. Tag signal width and height as a function of the passive component values. (a) Mean and standard deviation of measured tag signal width versus C_w , and (b) mean and standard deviation of measured tag signal height versus R_{h2} .

height of the tag signal required to distinguish the adjacent pixel. The spread of the measured tag width was consistently independent of the component value, but the tag signal height slightly increased with increasing R_{h2} . However, the maximum spread within the measurement range was less than 9 mV when R_{h2} was 51 Ω . For the clear separation of each SiPM pixel, the spacing between adjacent pixels was set to at least 5 times that of the minimum spacing (1 ns for width and 50 mV for height, see section 2.3).

3.2. Block detector performance

The performance of block detector including crystal identification accuracy, energy resolution and time resolution was evaluated. The sixteen 3 mm crystals were clearly separated in the crystal-positioning map without overlap between adjacent crystals as shown in figure 8(a). The average DWRs in the x and y -direction were 12.27 ± 2.84 and 7.36 ± 2.07 , respectively.

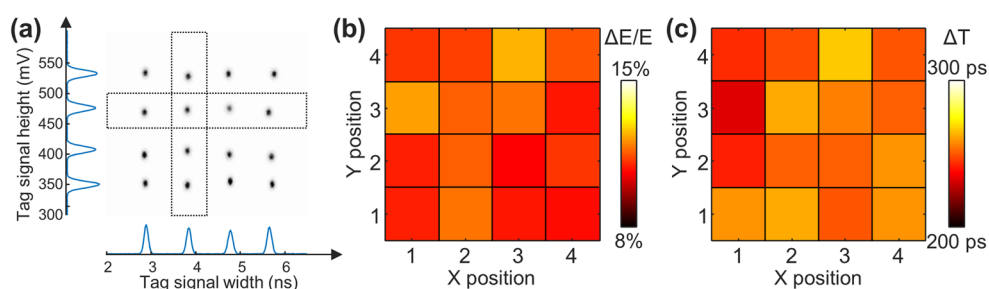


Figure 8. Block detector performance using PTM circuit at <10 kcps. (a) Crystal-positioning map and profiles of selected row and column, (b) energy resolution distribution and (c) CRT distribution.

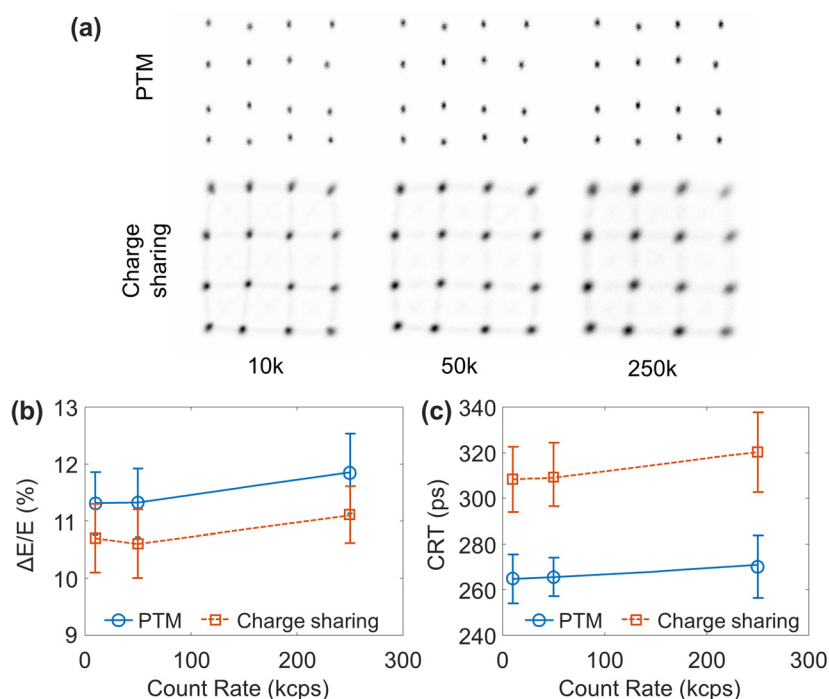


Figure 9. Changes in detector performance at different single count rates. (a) Crystal-positioning map, (b) energy resolution, and (c) CRT.

Figures 8(b) and (c) show the energy resolution and CRT distribution of PTM detector. The average energy resolution for 511 keV gamma-ray and CRT of the 16 scintillation crystals were $11.31 \pm 0.55\%$ and 264.7 ± 10.7 ps, respectively.

Figure 9 shows the experimental results at different count rates. The increase of the single count rate in the PTM method had negligible effect on the quality of the crystal-positioning map because the position in the map was solely determined by the short tag signal (<6 ns in this study). However, the count rate increase had considerable effect on the crystal-positioning map of the charge sharing method because the map was composed by the ratio of the charge integration for a relatively long period (~150 ns), thus being more vulnerable to the pulse pile up problem.

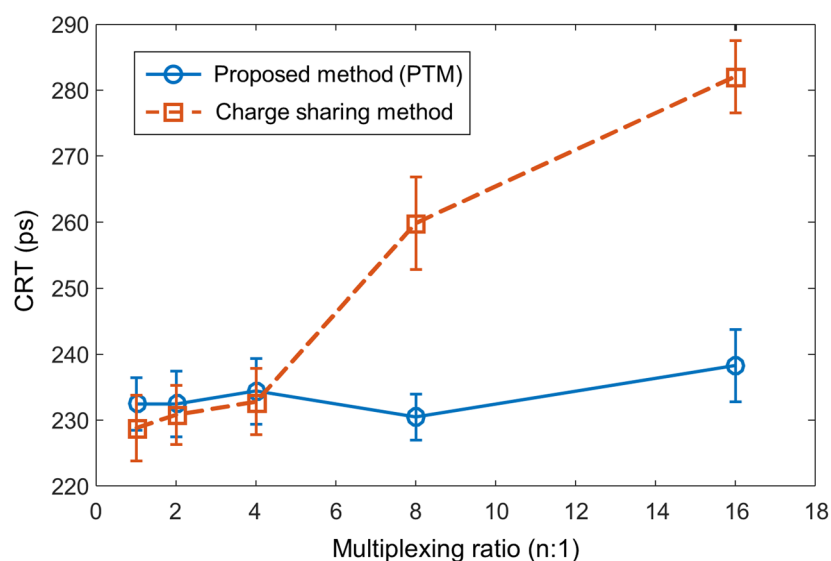


Figure 10. CRT as a function of the multiplexing ratio.

The energy resolution and CRT were degraded as the count rate increased for both PTM and charge sharing detectors because the probability of pulse pile up increases at high count rates. Nevertheless, both detectors maintained good performance levels even at a high counting rate of 250 kcps.

3.3. Time resolution as a function of multiplexing ratio

Figure 10 shows the CRT as a function of multiplexing ratio. If the multiplexing ratio was less than or equal to 4, CRT of the PTM method was slightly degraded compared to charge sharing method. This is because of the additional timing jitter from the PTM circuit components such as the comparator, digital logic gates, and summing amplifier. If the multiplexing ratio was greater than 4, CRT of the charge sharing method would rapidly degrade by the accumulating dark current. In contrast, the PTM method kept constant CRT (~232 ps) even for a multiplexing ratio of 16:1.

The time resolution obtained in this study was better than that obtained from the 4×4 block detector (section 3.2) despite the same temperature and bias voltage, because the array suffered crosstalk between adjacent crystal pixels and imperfect matching between the crystals and the SiPM pixels (Yeom *et al* 2013a).

All of the evaluations were performed at 20 °C, but several recent studies reported that there is little dependence of the CRT on the temperature (Yeom *et al* 2013b, Nemallapudi *et al* 2015).

3.4. Feasibility of DOI measurement

The ratio of tail integration to head integration was calculated to distinguish two LGSO crystals.

The two types of LGSO crystals are clearly identified in the pulse shape spectra as shown in figure 11. The peak-to-valley ratio was 8.4, thanks to the well preserved shape information in the scintillation pulse with the tagged signal.

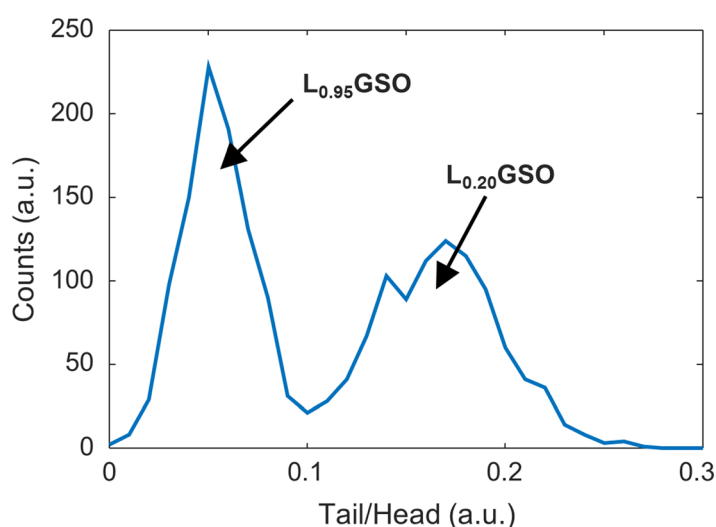


Figure 11. Pulse shape analysis of phoswich detector consisting of $L_{0.95}\text{GSO}$ and $L_{0.20}\text{GSO}$.

4. Discussion and conclusion

Several effective ways to reduce the number of readout channels in PET detectors have been suggested in previous studies. In these studies, the signals from multiple photosensors were directly or weighted summed to estimate photon interaction position. However, these methods are not suitable for fast response time particularly for large area SiPM arrays because the increase in multiplexing ratio leads to an increase in the accumulation of dark current and capacitance. In this study, we proposed a new multiplexing method and showed that this method does not degrade the timing performance as the multiplexing ratio is increased.

We evaluated the detector performance of the PTM and compared it with the conventional charge sharing method at different count rates. Because very short square pulses (<6 ns) were used for tagging, the count rate performance did not degrade significantly compared to the charge sharing method.

The CRT of the charge sharing method deteriorated with an increasing multiplexing ratio, while that of the PTM was kept almost constant. For the multiplexing ratio greater than 16, more rapid CRT deterioration is expected in charge sharing method due to the accumulation of more and more dark noise. However, the PTM method is likely to maintain timing performance for the larger array because the tag signals are generated individually.

Another advantage of the proposed method is that it required only one signal channel for acquiring a 2D photon interaction position, while most of the multiplexing methods require at least four signal channels for 2D mapping. A 4×4 crystal block was used for the proof-of-concept detector in which the area was smaller than the block detector used in conventional whole body PET, but it can easily be extended to large area detectors. Experimental results reveal that there is more room for additional steps with regard to the tag signal width and height. Without the degradation of the crystal-positioning map, i.e. keeping the step size of the tag signal width and height, the 8×8 detector or even larger arrays can be read out using a single channel output. For example, 64 SiPMs in the 8×8 detector can be encoded with an amplitude of 250, 300, 350, 400, 450, 500, 550, and 600 mV and a width of 3, 4, 5, 6, 7, 8, 9, and 10 ns. In this case, the crystal identifying performance would be similar to the 4×4

detector used in this paper. However, since the sensitivity of the 8×8 detector increases by approximately four times, a better counting performance is required. Therefore, the detector performance of the 8×8 detector would be worse than that of the 4×4 detector at the high count rate.

The timing resolution results in this paper are promising (~ 230 ps for a single pixel), but there is still room for improvement. Recently, several studies have demonstrated the advance in CRT for PET detectors using novel scintillator and SiPM photosensors. Cates and Levin (2016), for example, have reported exceptional CRT (~ 120 ps) in a single crystal bench top setup using a fast LGSO scintillator $\text{Lu}_{1.8}\text{Gd}_{0.2}\text{SiO}_4:\text{Ce}$ (0.025 mol% Ce concentration) that has similar light output with the standard LGSO used in this study but a 30% improved decay time. Nemallapudi *et al* (2015) have also reported 140 ps CRT using Ca co-doped LSO:Ce crystal which has improved scintillation properties than standard LSO:Ce (Weele *et al* 2015). In these two studies, novel near ultraviolet high density (NUV-HD) SiPM of Fondazione Bruno Kessler (FBK) was used. This new analog SiPM has higher photon detection efficiency and lower dark count rate than the SiPM used in this paper, which allows a better CRT.

We also showed the feasibility of this method for a DOI detector using PSD. However, some limitations are worth noting; the detector configuration used in this study is not suitable for TOF applications because the $\text{L}_{0.2}\text{GSO}$ has low light output and slow decay time. Better configurations for TOF applications have been studied by several groups using a $\text{LaBr}_3/\text{CeBr}_3$ pair (Schmall *et al* 2015) or an $\text{L}_{0.95}\text{GSO}$ -fast (0.025 mol% Ce)/ $\text{L}_{0.95}\text{GSO}$ -slow (0.75 mol% Ce) pair (Yamamoto *et al* 2016). Another possible approach is the use of a phosphor-coated single layer crystal to make the depth-dependent decay time different (Berg *et al* 2016). Future work should therefore include a DOI detector using the fast and bright scintillator pair to construct the DOI-TOF block.

In this study, we evaluated the feasibility of the PTM method using the digital oscilloscope. However, the use of oscilloscope is not a practical way for the system implementation due to cost and space issues. One reasonable approach would be to use a switched capacitor array such as the domino ring sampler 4 (DRS4). The DRS4-based data acquisition system can digitize the waveform with 5 GSa s^{-1} horizontal resolution and 12 bit vertical resolution (Ko and Lee 2015). Therefore, it can be extended to the system level using a DRS4-based digitizer with negligible performance degradation at a reasonable price.

In conclusion, the proposed multiplexing method allows decoding of the 3D interaction position of gamma rays in a scintillation detector with single line readout. Energy resolution, CRT, and pulse shape are well preserved showing promising TOF and DOI capability.

Acknowledgments

This work was supported by grants from the National Research Foundation of Korea (NRF), funded by the Korean Ministry of Science, ICT and Future Planning (grant no. NRF-2014M3C7034000 and NRF-2016R1A2B3014645), and the Korea Health Technology R&D Project through the Korea Health Industry Development Institute (KHIDI), funded by the Ministry of Health and Welfare, Republic of Korea (grant no. HI14C1135).

References

- Aguilar A, Gonzalez A J, Torres J, García-Olcina R, Martos J, Soret J, Conde P, Hernández L, Sánchez F and Benlloch J M 2015 Timing results using an FPGA-based TDC with large arrays of 144 SiPMs *IEEE Trans. Nucl. Sci.* **62** 12–8

- Becker R *et al* 2016 The SAFIR experiment: Concept, status and perspectives *Nucl. Instrum. Methods Phys. Res.* at press (DOI: [10.1016/j.nima.2016.05.037](https://doi.org/10.1016/j.nima.2016.05.037))
- Berg E, Roncali E, Kapusta M, Du J and Cherry S R 2016 A combined time-of-flight and depth-of-interaction detector for total-body positron emission tomography *Med. Phys.* **43** 939–50
- Cates J W and Levin C S 2016 Advances in coincidence time resolution for PET *Phys. Med. Biol.* **61** 2255–64
- Cates J W, Vinke R and Levin C S 2015 Analytical calculation of the lower bound on timing resolution for PET scintillation detectors comprising high-aspect-ratio crystal elements *Phys. Med. Biol.* **60** 5141–61
- Conti M 2010 Why is TOF PET reconstruction a more robust method in the presence of inconsistent data? *Phys. Med. Biol.* **56** 155–68
- Conti M 2011 Focus on time-of-flight PET: the benefits of improved time resolution *Eur. J. Nucl. Med. Mol. Imaging* **38** 1147–57
- Conti M, Eriksson L and Westerwoudt V 2013 Estimating image quality for future generations of TOF PET scanners *IEEE Trans. Nucl. Sci.* **60** 87–94
- Downie E, Yang X and Peng H 2013 Investigation of analog charge multiplexing schemes for SiPM based PET block detectors *Phys. Med. Biol.* **58** 3943–64
- Gola A, Piemonte C and Tarolli A 2013 Analog circuit for timing measurements with large area SiPMs coupled to LYSO crystals *IEEE Trans. Nucl. Sci.* **60** 1296–302
- Grant A M and Levin C S 2014 A new dual threshold time-over-threshold circuit for fast timing in PET *Phys. Med. Biol.* **59** 3421–30
- Gundacker S, Auffray E, Frisch B, Jarron P, Knapitsch A, Meyer T, Pizzichemi M and Lecoq P 2013 Time of flight positron emission tomography towards 100ps resolution with L(Y)SO: an experimental and theoretical analysis *J. Instrum.* **8** P07014
- Ito M, Hong S J and Lee J S 2011 Positron emission tomography (PET) detectors with depth-of-interaction (DOI) capability *Biomed. Eng. Lett.* **1** 70–81
- Jung J H, Choi Y and Im K C 2016 PET/MRI: technical challenges and recent advances *Nucl. Med. Mol. Imaging* **50** 3–12
- Kang H G, Hong S J, Ko G B, Yoon H S, Song I C, Rhee J T and Lee J S 2015 Assessment of MR-compatibility of SiPM PET insert using short optical fiber bundles for small animal research *J. Instrum.* **10** P12008
- Ko G B and Lee J S 2015 Performance characterization of high quantum efficiency metal package photomultiplier tubes for time-of-flight and high-resolution PET applications *Med. Phys.* **42** 510–20
- Ko G B, Kim K Y, Yoon H S, Lee M S, Son J-W, Im H J and Lee J S 2016a Evaluation of a silicon photomultiplier PET insert for simultaneous PET and MR imaging *Med. Phys.* **43** 72–83
- Ko G B, Yoon H S, Kim K Y, Lee M S, Yang B Y, Jeong J M, Lee D S, Song I C, Kim S, Kim D and Lee J S 2016b Simultaneous multi-parametric PET/MRI with silicon photomultiplier PET and ultra-high field MRI for small animal imaging *J. Nucl. Med.* **57** 1309–15
- Ko G B, Yoon H S, Kwon S I, Lee C M, Ito M, Hong S J, Lee D S and Lee J S 2013 Development of a front-end analog circuit for multi-channel SiPM readout and performance verification for various PET detector designs *Nucl. Instrum. Methods Phys. Res. A* **703** 38–44
- Lee J S and Kim J H 2014 Recent advances in hybrid molecular imaging systems *Semin. Musculoskelet. Radiol.* **18** 103–22
- Levin C S, Maramraju S H, Khalighi M M, Deller T W, Delso G and Jansen F 2016 Design features and mutual compatibility studies of the time-of-flight PET capable GE SIGNA PET/MR System *IEEE Trans. Med. Imaging* **35** 1907–14
- Liu C Y and Goertzen A L 2014 Multiplexing approaches for a 12×4 array of silicon photomultipliers *IEEE Trans. Nucl. Sci.* **61** 35–43
- Liu C and Wang Y 2015 A 128 channel, 710 M samples/second, and less than 10ps RMS resolution time-to-digital converter implemented in a Kintex-7 FPGA *IEEE Trans. Nucl. Sci.* **62** 773–83
- Miller M, Zhang J, Binzel K, Griesmer J, Laurence T, Narayanan M, Natarajamani D, Wang S and Knopp M 2015 Characterization of the vereos digital photon counting PET system *J. Nucl. Med.* **56** 434
- Neill K O and Jackson C 2015 SensL B-Series and C-Series silicon photomultipliers for time-of-flight positron emission tomography *Nucl. Instrum. Methods Phys. Res. A* **787** 169–72
- Nemallapudi M V, Gundacker S, Lecoq P, Auffray E, Ferri A, Gola A and Piemonte C 2015 Sub-100ps coincidence time resolution for positron emission tomography with LSO: Ce codoped with Ca *Phys. Med. Biol.* **60** 4635–49

- Nishikido F, Obata T, Shimizu K, Suga M, Inadama N, Tachibana A, Yoshida E, Ito H, Yamaya T 2014 Feasibility of a brain-dedicated PET-MRI system using four-layer DOI detectors integrated with an RF head coil *Nucl. Instrum. Methods Phys. Res. A* **756** 6–13
- Olcott P, Kim E, Hong K, Lee B J, Grant A M, Chang C-M, Glover G, Levin C S 2015 Prototype positron emission tomography insert with electro-optical signal transmission for simultaneous operation with MRI *Phys. Med. Biol.* **60** 3459–78
- Pepin C M, Bérard P, Perrot A L, Pépin C, Houde D, Lecomte R, Melcher C L and Dautet H 2004 Properties of LYSO and recent LSO scintillators for phoswich PET detectors *IEEE Trans. Nucl. Sci.* **51** 789–95
- Powolny F *et al* 2011 Time-based readout of a silicon photomultiplier (SiPM) for time of flight positron emission tomography (TOF-PET) *IEEE Trans. Nucl. Sci.* **58** 597–604
- Roncali E, Phipps J E, Marcu L and Cherry S R 2012 Pulse shape discrimination and classification methods for continuous depth of interaction encoding PET detectors *Phys. Med. Biol.* **57** 6571–85
- Schmall J P, Surti S and Karp J S 2015 Characterization of stacked-crystal PET detector designs for measurement of both TOF and DOI *Phys. Med. Biol.* **60** 3549–65
- Schmall J P, Wiener R I, Surti S, Ferri A, Gola A, Tarolli A, Piemonte C and Karp J S 2014 Timing and energy resolution of new near-UV SiPMs coupled to: Ce for TOF-PET *IEEE Trans. Nucl. Sci.* **61** 2426–32
- Schmand M, Eriksson L, Casey M E, Andreaco M S, Melcher C, Wienhard K, Flugge G and Nutt R 1998 Performance results of a new DOI detector block for a high resolution PET-LSO research tomograph HRRT *IEEE Trans. Nucl. Sci.* **45** 3000–6
- Seifert S and Schaart D R 2015 Improving the time resolution of TOF-PET detectors by double-sided readout *IEEE Trans. Nucl. Sci.* **62** 3–11
- Seifert S, Van der Lei G, Van Dam H T, Schaart D R 2013 First characterization of a digital SiPM based time-of-flight PET detector with 1 mm spatial resolution *Phys. Med. Biol.* **58** 3061–74
- Shimazoe K, Takahashi H, Shi B, Orita T, Furumiya T, Ooi J and Kumazawa Y 2012 Dynamic time over threshold method *IEEE Trans. Nucl. Sci.* **59** 3213–7
- Song T Y, Wu H, Komarov S, Siegel S B and Tai Y C 2010 A sub-millimeter resolution PET detector module using a multi-pixel photon counter array *Phys. Med. Biol.* **55** 2573–87
- Surti S 2015 Update on time-of-flight PET imaging *J. Nucl. Med.* **56** 98–105
- Traxler M, Bayer E, Kajetanowicz M, Korcyl G, Maier L, Michel J, Palka M and Ugur C 2011 A compact system for high precision time measurements (<14 ps RMS) and integrated data acquisition for a large number of channels *J. Instrum.* **6** C12004
- Ullah M N, Pratiwi E, Cheon J, Choi H, Yeom J Y 2016 Instrumentation for time-of-flight positron emission tomography *Nucl. Med. Mol. Imaging* **50** 112–22
- Weele D N, Schaart D R, and Dorenbos P 2015 Comparative study of co-doped and non co-doped LSO:Ce and LYSO:Ce scintillators for TOF-PET *IEEE Trans. Nucl. Sci.* **62** 727–31
- Wehner J, Weissler B, Dueppenbecker P M, Gebhardt P, Goldschmidt B, Schug D, Kiessling F, Schulz V 2015 MR-compatibility assessment of the first preclinical PET-MRI insert equipped with digital silicon photomultipliers *Phys. Med. Biol.* **60** 2231–55
- Won J Y, Kwon S I, Yoon H S, Ko G B, Son J W and Lee J S 2015 Dual-phase tapped-delay-line time-to-digital converter with on-the-fly calibration implemented in 40 nm FPGA *IEEE Trns. Biomed. Circuits Syst.* **10** 231–42
- Yamamoto S, Kobayashi T, Okumura S and Yeom J Y 2016 Timing performance measurements of Si-PM-based LGSO phoswich detectors *Nucl. Instrum. Methods Phys. Res.* **821** 101–8
- Yamamoto S, Watabe T, Watabe H, Aoki M, Sugiyama E, Imaizumi M, Kanai Y, Simosegawa E and Hatazawa J 2012 Simultaneous imaging using Si-PM-based PET and MRI for development of an integrated PET/MRI system *Phys. Med. Biol.* **57** N1–13
- Yeom J Y, Vinke R, and Levin C S 2013b Optimizing timing performance of silicon photomultiplier-based scintillation detectors *Phys. Med. Biol.* **58** 1207–20
- Yeom J Y, Vinke R, Spanoudaki V C, Hong K J and Levin C S 2013a Readout electronics and data acquisition of a positron emission tomography time-of-flight detector module with waveform digitizer *IEEE Trans. Nucl. Sci.* **60** 3735–41
- Yoon H S, Ko G B, Kwon S I, Lee C M, Ito M, Song I C, Lee D S, Hong S J and Lee J S 2012 Initial results of simultaneous PET/MRI experiments with an MRI-compatible silicon photomultiplier PET scanner *J. Nucl. Med.* **53** 608–14